AGU PUBLICATIONS

JGR

Journal of Geophysical Research: Biogeosciences

RESEARCH ARTICLE
10.1002/2013JG002493

Key Points:
- The first global seasonal understory reflectivity maps
- Mapping understory reflectivity with MISR data
- Help to model contributions of forest and understory vegetation in ecosystem

Correspondence to:
R. Liu,
liurg@igsnrr.ac.cn

Citation:
Jiao, T., R. Liu, Y. Liu, J. Pisek, and J. M. Chen (2014), Mapping global seasonal forest background reflectivity with Multi-angle Imaging Spectroradiometer data, *J. Geophys. Res. Biogeosci.*, *119*, 1063–1077, doi:10.1002/2013JG002493.

Received 27 AUG 2013
Accepted 3 MAY 2014
Accepted article online 10 MAY 2014
Published online 9 JUN 2014

Mapping global seasonal forest background reflectivity with Multi-angle Imaging Spectroradiometer data

Tong Jiao[1], Ronggao Liu[1], Yang Liu[1], Jan Pisek[2], and Jing M. Chen[3,4]

[1]LREIS, Institute of Geographic Sciences and Natural Resources Research, Chinese Academy of Sciences, Beijing, China, [2]Tartu Observatory, Tõravere, Estonia, [3]Nanjing University, Nanjing, China, [4]Department of Geography, University of Toronto, Toronto, Ontario, Canada

Abstract Forest background reflectivities with seasonal and spatial variations are critically important in the estimation of canopy biophysical parameters of the forest canopy. In this paper, seasonal background reflectivity for global forested areas was mapped at 1.1 km resolution using four-scale model and Multi-angle Imaging Spectroradiometer data of the nadir and 45° forward directions. The largest seasonal variation of forest background reflectivities was observed in middle and high latitudes of Northern Hemisphere. The background reflectivity differs between deciduous broadleaf forest and coniferous forest in the near-infrared band and varies with increasing canopy leaf area index. The partial validation of forest background reflectivity with adjacent grassland in the Northern Hemisphere and the comparison of understory leaf area index on leaf appearance day for larch forest in North Asia both indicate the relative reliability of results. The nearly 70% spatial coverage of retrieval with high-quality flags makes it eligible for applications over global coniferous and deciduous broadleaf forest areas.

1. Introduction

Forests play a critically important role in the exchange of energy, water, and carbon between continents and the atmosphere [*Sellers et al.*, 1997]. Quantitative descriptions of forest have been regarded as the key parts to quantify cycles of carbon and water. Leaf area index (LAI) is one of the most important parameters in characterizing forest structure and its energy absorption capacity. Remote sensing capable of monitoring the environment at a continental or global scale over periods of multiple years provides the only access to quantify these geophysical parameters at large scales with spatial and temporal continuity [*Pinty et al.*, 2008], which provides a powerful tool for modeling of climate, hydrology, and ecology [*Diner et al.*, 2005]. However, the retrieval of these biophysical properties of the forest canopy layer is complicated by the often dominating role of the forest background in spectral signal [*Chen and Cihlar*, 1996; *Eriksson et al.*, 2006; *Rautiainen*, 2005; *Spanner et al.*, 1990], particularly when forests have open canopies or low density, or observation angles are close to the nadir. In addition, the lack of information about forest background would introduce large uncertainties in modeling forest canopy reflectance and in interpreting the measured reflectance spectra [*Ahl et al.*, 2006; *Eriksson et al.*, 2006; *Wang et al.*, 2004]. For example, the overestimation of LAI in many global products would mainly be attributed to the limited optical information about understory vegetation [*Garrigues et al.*, 2008; *Kobayashi et al.*, 2010].

Forest background defined here refers to all the materials below the forest canopy, such as understory vegetation, rock, soil, leaf litter, lichen, moss, snow, or their mixture [*Pisek and Chen*, 2009]. Considerable efforts have been spent to find a suitable method to compensate for the influence of forest background in estimating canopy LAI. One approach is to design a special vegetation index which aims at estimating forest canopy biophysical properties through enhancing the spectral contribution of overstory vegetation while minimizing that of the underlying soil or understory vegetation [e.g., *Brown et al.*, 2000; *Gonsamo and Pellikka*, 2012; *Huete*, 1988; *Nemani et al.*, 1993; *Qi et al.*, 1994]. Even though many of the indices are considered to diminish to a certain extent, the background effect in the relationship between canopy LAI and total reflectance, their dependence on the relative contributions of the ground and tree layer component which differ along with sensor and Sun angles [*Rautiainen*, 2005], strongly limits their applications at large scales. Another approach assumes that the background is mainly composed of one or two components and uses

measured spectral libraries of common background components such as shrub, grass, lichen, and moss [e.g., *Lang et al.*, 2002; *Miller et al.*, 1997; *Peltoniemi et al.*, 2005; *Rautiainen et al.*, 2007; *Rees et al.*, 2004] as input in forest canopy models. However, the limited spectral libraries would not represent well the optical properties of real forest background which often has highly spatial and temporal variations [*Peltoniemi et al.*, 2005; *Rautiainen et al.*, 2011]. The misrepresentation of forest background would finally result in great uncertainty in the retrieved canopy LAI. It is should be a better approach to use a background reflectance derived from satellite data as a direct input for forest canopy models.

It is nearly impossible to retrieve background reflectivity directly from monoangle satellite data because the number of unknown parameters both from the background and the canopy exceeds the number of measurements [*Gemmell*, 2000]. Although there are multispectral observations, for each band, there is one additional unknown parameter, i.e., the background reflectance in that band. And it is difficult to build relationships between reflectances in different bands due to the complex composition of forest background. Compared with the single-angle data, multi-angle data provide more information for the separation of forest background from forest canopy [*Chopping*, 2008]. Under the assumption that forest background is homogeneous, its reflectance in a given spectral band does not change much with the viewing zenith angle while its contribution to the total reflectance differs along with the observation zenith angle on oblique plane from the principle solar plane in a predictable manner. In addition, the reflectance of overstory will change little with the viewing zenith angle and its small change could be considered in forest reflectance models. Consequently, the inversions using multi-angle spectral data allow the background reflectances to be included in the inversion process. Forest background reflectivity over forest areas of North America has been mapped at 1° spatial resolution by using two view angles' observation from MISR (Multi-angle Imaging Spectroradiometer) [*Pisek and Chen*, 2009]. Its incorporation into a global LAI algorithm has been shown to significantly improve the estimation of canopy LAI over boreal forest areas [*Pisek et al.*, 2010].

In this paper, we intend (a) to map the global seasonal forest background reflectivity at 1.1 km resolution, (b) to examine the optical properties and seasonal changes of the forest background over global coniferous and deciduous broadleaf forest areas, (c) to validate forest background reflectivities over Northern Hemisphere, and (d) to evaluate the performance of the algorithm under different canopy LAI and the eligibility of results for global applications.

2. Data

2.1. MISR Data

The MISR on board the Earth Observing System satellite, Terra, is capable of observing the Earth's surface from nine different angles and obtaining images at four spectral bands for each view direction. The nine view angles consist of four forward directions (denoted as Af, Bf, Cf, and Df in the order of increasing off-nadir angle), four afterward directions (Aa, Ba, Ca, and Da), and a nadir direction (An). The nominal view angles from nadir to the two directions are 0°, ± 26.1°, ± 45.6°, ± 60.0°, and ± 70.5°. The four bands are blue (centered at 446 nm; bandwidth 42 nm), green (558 nm; 29 nm), red (672 nm, 22 nm), and near-infrared (NIR) (866 nm; 40 nm) [*Diner et al.*, 1998].

The daily MISR data employed in this study cover global continents from 2000 to 2010. The data include MISR Level 2 MIL2ASLS land surface parameters (surface bidirectional reflectance factor (BRF)), MISR Level 1B2 MI1B2GEOP geometric parameters (Sun/view and zenith/azimuth angles), and MISR ancillary geographic products (longitude and latitude of pixels). MISR Level 2 products are resampled to 1100 m resolution and screened for contamination from sources such as clouds, cloud shadows, Sun glitter over water, topographically complex terrain, and topographically shadowed regions [*Bothwell et al.*, 2002]. All data were provided in the Space Oblique Mercator projection and can be downloaded from https://eosweb.larc.nasa.gov/order-data.

2.2. Ancillary Data

The forest types were obtained from the Moderate Resolution Imaging Spectroradiometer (MODIS) land cover product (MCD12Q1), and the initial LAI series were provided by GLOBMAP LAI [*Liu et al.*, 2012].

The MCD12Q1 product provides a yearly 500 m land cover classification map of the global area and is derived through a supervised decision tree classification with five different classification schemes. In this study, the Land Cover Type 3 (LAI/fraction of photosynthetically active radiation) classification scheme product is

selected, which includes eight natural vegetation classes, one nonvegetated land class, and one urban class. The global forest areas (our study area) are classified into four biome types in this product including evergreen broadleaf forest, evergreen needleleaf forest, deciduous broadleaf forest, and deciduous needleleaf forest. The MCD12Q1 product in 2001 was chosen to represent global land cover in all years of data retrieval. The MCD12Q1 is provided in a sinusoidal grid and downloaded from https://lpdaac.usgs.gov/.

The GLOBMAP LAI series from 2000 to 2010 contain a global 8 day composite true LAI of the land surface in a 500 × 500 m grid [*Liu et al.*, 2012]. It was derived from the MOD09A1 land surface reflectance and illumination and view angles data through the GLOBCARBON LAI algorithm [*Deng et al.*, 2006]. This algorithm relies on the land cover-dependent relationships between LAI and the simple ratio (SR) as well as reduced simple ratio with the consideration of bidirectional reflectance distribution function (BRDF) effects explicitly. The LAI product can be downloaded from the Web site (http://www.globalmapping.org/globalLAI).

3. Methodology

3.1. Retrieval of Background Reflectivity

The forest stand viewed by sensors can be divided into canopy and background components, each of which has sunlit and shaded components. As single scattering is the dominant part of total reflectance over sparse forest areas [*Rautiainen et al.*, 2004, 2008b; *Roujean et al.*, 1992], where the effect of background is pronounced, the total reflectance of a pixel can be then expressed as a linear combination of proportional reflectances [*Bacour and Breon*, 2005; *Chen et al.*, 2000; *Chopping*, 2008; *Li and Strahler*, 1985]:

$$R = R_T K_T + R_G K_G + R_{ZT} K_{ZT} + R_{ZG} K_{ZG} \tag{1}$$

where R_T, R_G, R_{ZT}, and R_{ZG} are the reflectances of the sunlit crown, sunlit background, shaded crown, and shaded background, respectively, and the K for each R denotes its proportion in the instantaneous field-of-view. Assuming that the reflectance of canopy and background at a given illumination angle changes little with chosen view angles, background reflectance can be resolved with two observations angles. It has been shown that the directional dependence of canopy reflectance factors is the greatest in the principal solar plane and decreases fast as the viewing azimuth angle moves away from this plane [*Bicheron et al.*, 1997; *Peltoniemi et al.*, 2005; *Sandmeier and Deering*, 1999]. MISR, a multiple sensor which observes the Earth in an oblique plane, provides suitable observation condition on which the influence of BRDF is reduced [*Diner et al.*, 2002]. The measurements of directional reflectances of forest floor indicate that the azimuthal dependence of the reflectance is not so strong [*Peltoniemi et al.*, 2005] and the reflectance in forward scattering direction changes little in different zenith angles [*Bacour and Breon*, 2005; *Kaasalainen and Rautiainen*, 2005]. The nadir reflectance, Rn, and oblique reflectance, Ra, are stated as follows:

$$R_n = R_T K_{Tn} + R_G K_{Gn} + R_{ZT} K_{ZTn} + R_{ZG} K_{ZGn} \tag{2}$$

$$R_a = R_T K_{Ta} + R_G K_{Ga} + R_{ZT} K_{ZTa} + R_{ZG} K_{ZGa} \tag{3}$$

According to the study of *Pisek et al.* [2009], the reflectivities of shaded crown and ground (i.e., R_{ZT} and R_{ZG}) are dynamically expressed as functions of their sunlit part and the multiple scattering factor [*White et al.*, 2001, 2002a, 2002b], giving $R_{ZT} = MR_T$ and $R_{ZG} = MR_G$ where $M = R_Z/R$ for a reference target. Solving equations (2) and (3), forest background reflectance is then expressed as follows:

$$R_G = \frac{R_n(K_{Ta} + K_{ZTa}M) - R_a(K_{ZTn}M + K_{Tn})}{K_{Gn}K_{Ta} - K_{Tn}K_{Ga} + M(K_{Gn}K_{ZTa} - K_{Tn}K_{ZGa} + K_{Ta}K_{ZGn} - K_{Ga}K_{ZTn}) + M^2(K_{ZGn}K_{ZTa} - K_{ZTn}K_{ZGa})} \tag{4}$$

where the total reflectances R_n and R_a are acquired from the nadir and chosen angle observation of MISR, M is treated as angular-independent, wavelength-dependent constant predetermined in the inversion [*Chen and Leblanc*, 1997], and the K proportions were predicted from the four-scale model.

3.2. Estimating Probabilities of Viewing Sense Components

The proportions of the components in equation (4) are calculated using the four-scale model [*Chen and Leblanc*, 1997, 2001; *Leblanc et al.*, 1999]. This is a geometric-optical radiative-transfer model with an emphasis on canopy architecture at four scales including tree groups, tree crowns, branches, and shoots or leaves. Several important properties of the four-scale model in estimating the proportions are the following:

Table 1. Input Parameters to Four-Scale

Parameter	Unit	Coniferous	Deciduous
Stand density	Trees/ha	1000, 2000, 3000	1000, 2000, 3000
Clumping index (Ω_E)		0.7	0.8
Tree shape		Cone + cylinder	Spheroid
Crown base height	m	4	5
Crown vertical dimension	m	12	15
Crown radius	m	0.75	2

1. The spatial distribution of trees is considered to be nonrandom and is stimulated using the Neyman type A distribution [*Neyman*, 1939]. The mutual shadowing between tree crowns is considered using a negative binomial and the Neyman distribution theory together with natural repulsion effect.
2. The crowns are stimulated as discrete geometrical objects: cone and cylinder for conifers, and spheroid for deciduous species, both of which are found to be effective in capturing the BRDF effect on canopy reflectance [*Rautiainen et al.*, 2004, 2008a].
3. The tree crown surface is treated as a complex medium within which mutual shadowing occurs so that shadowed foliage can be observed on the sunlit side and sunlit foliage on the shaded side.

Although the four-scale model requires many input parameters, it remains a powerful tool with a set of general parameters fixed [*Canisius and Chen*, 2007]. According to the simulation by *Nilson and Peterson* [1994], the main factors required in geometric-optical modeling of stand reflectances include LAI, canopy closure, tree type, and background reflectivity while parameters like stand density, tree height, and tree stem diameter were less important. Thus, the values for these tree architectural parameters of coniferous and deciduous types were fixed in the four-scale model inversion (Table 1). The parameters such as LAI, solar and view zenith angles (SZA and VZA), the relative azimuth angle between the Sun and the viewing camera (PHI) varied between pixels. These parameters could be obtained from the satellite images as described in the data section.

Running four-scale model on multi-angle images pixel by pixel at a global scale is computationally impractical, and therefore, the method of look-up tables (LUTs) was applied for image processing. Different from the 10 LUTs adopted by the previous study over North America [*Pisek and Chen*, 2009], only six of them, three for the coniferous and deciduous forest type each, were used so as to reduce the data processing time. Ranges of values agree with the original LUT dimensions of *Canisius and Chen* [2007]: LAI from 0.1 to 10, SZA from 0° to 70°, PHI from 100° to 170° along with the nominal VZA of MISR cameras. The forest densities represented by the three LUTs for each forest type are 1000, 2000, and 3000 trees/ha, respectively. As the performance of the background reflectivity algorithm was shown not to be sensitive to the assumed stand density in case of low to intermediate densities [*Pisek et al.*, 2009] where the effect of the background reflectance on the total canopy signal is the greatest [*Rautiainen et al.*, 2007], the background reflectivity is finally calculated as an average value of the three results predicted with MISR data, multiple scattering factor *M* and component fractions retrieved from LUTs for the three different stand densities for the given biome (Table 1).

3.3. Data Processing

Data used for retrieval were first preprocessed to the geographic coordinate. MISR BRF (An, Bf, and Ba cameras) and GLOBMAP LAI data sets from 2000 to 2010, and MCD12Q1 product in 2001 were transformed to geographic projection at 0.01° × 0.01° spatial resolution by nearest neighbor interpolation. MISR geometric parameters product was reprojected to a 0.16° × 0.16° grid data set. All the processed data were combined to form global maps.

A C language code was developed to read the preprocessed data and compute background reflectivity from two angular images of MISR. The two view zenith angles chosen in this study agree with that used by *Pisek and Chen* [2009]: the nadir and 45.6° camera (Bf). These smaller view angles not only increase the proportions of background being observed but also avoid the slight increase of BRF of the crown in larger view angles in the forward scattering direction particularly for broadleaf species [*Deering et al.*, 1999]. In addition, *Pisek et al.* [2009] indicates that background reflectivity retrievals at smaller view zenith angles are slightly more accurate.

The C code ran with daily data on a global scale from 2000 to 2010. The background reflectivities were retrieved at the spatial resolution of 1.1 km for the red and the NIR bands of MISR so that the absorption and scattering of understory vegetation could be best illustrated. Accompanying the retrieval of forest background reflectivity, a quality assessment based on the quality of input parameters, i.e., BRF, and LAI and the validity of retrieved background reflectivity was carried out to facilitate the evaluation of these algorithms. The states of input parameters (BRF and LAI) include invalid input, completely valid input, and partially valid input, and the retrieved results are classified as success or failure depending on the valid range of reflectance (0–1). There are generally three situations: (1) When the BRF data are invalid, the quality flag will be marked as "no retrieval." (2) When BRF is valid while LAI value is not valid, the LAI value will be first replaced by a value calculated from biome-dependent empirical relationship. Then, if retrieved results are within the valid range of reflectance, the quality flag will be marked by "valid retrieval," or it will be marked by "invalid retrieval." (3) When both the inputs are valid, the retrieval results will be marked by "high quality" only if the retrieved background reflectivity is valid. But if the retrieved background reflectivity is not within the range of reflectance, the retrieval will be marked by "invalid retrieval."

The low spatial and temporal coverage of retrieval caused by severe missing of MISR Land Surface Products had been observed in previous study over North America in 2007 [*Pisek and Chen*, 2009]. Similar problem also occurs in this study when only the results for a single year were included (not shown here). To illustrate the seasonal and spatial variations of global forest background reflectivity, it is essential to generate spatially coherent maps at a temporal step less than a season. An alternative strategy of filling the missing results suggested by Pisek [*Pisek and Chen*, 2009] is to assemble multi-year time series of retrieval results. Therefore, monthly combination of multi-year results at original spatial resolution ($0.01° \times 0.01°$) was adopted to produce maps of global forest background reflectivity in this study.

4. Results

4.1. Global Seasonal Forest Background Reflectivity Maps

Global forest background reflectivity in the red band shows a wide yearly range from 0.01 to 0.4 (Figure 1a). The most significant spatial difference appears during the period from January to March. The high reflectance of snow in understory in northern high latitudes creates a clear contrast with the low reflectance of understory vegetation, litters, or bare soil in lower latitudes. This high reflectance could be observed until April and is similar to the spectra measurements of the boreal forest understory at some northern sites in Canada [*Miller et al.*, 1997]. The spatial differences then begin to diminish in May because snow thaws and soil or evergreen vegetation with lower red reflectance becomes visible. From June to September, Northern Hemisphere forest background reflectance seems to be stable and dominates the lowest range of 0–0.05 in the red band due to the strong absorption by green vegetation [*Heiskanen*, 2006]. Spectral measurements of the European sub-boreal forest floor at this time periods also observed similar reflectance range in the red band for a variety of understory components such as dwarf shrub, dense or sparse grasses, and saplings [*Lang et al.*, 2002]. When the senescence period begins, red reflectance increases in northern high-latitude regions. Eastern Siberia, for example, experiences the earliest rising in red reflectance in October, and such high reflectance does not disappear until May of the following year as a result of thick snow cover throughout its winter [*Suzuki et al.*, 2001]. Southern Hemispheric variation in red reflectance is weaker than that occurring north of the Equator. Its value varies in an interval between 0.05 and 0.2. The continued cover of understory vegetation in a year [*Augspurger and Bartlett*, 2003; *Boyle and Bronstein*, 2012] may account for this small variation.

Global forest background reflectivity maps in the NIR band are shown in Figure 1b. The most dramatic seasonal variation of the background reflectance over northern high latitudes could be observed in autumn (from September to November). The lowest NIR reflectance in a year may be the results of litter cover and the inhibited growth of understory plants such as feather mosses [*Startsev et al.*, 2008]. In contrast, the transition from winter to spring in such regions is difficult to detect because snow and evergreen vegetation that compose the background for these two periods share similar reflectance in the NIR band. In summer, NIR reflectance increases with the color changing from light green to bright green in temperate regions of the Northern Hemisphere. This may be due to the enhanced scattering from cell-air-water interfaces inside the leaf during understory vegetation development when the total above ground water content in the herb and moss canopies increases dramatically [*Hallik et al.*, 2009]. In addition, some differences could also be observed between high- and middle-latitude regions in eastern Asia and North America at this time.

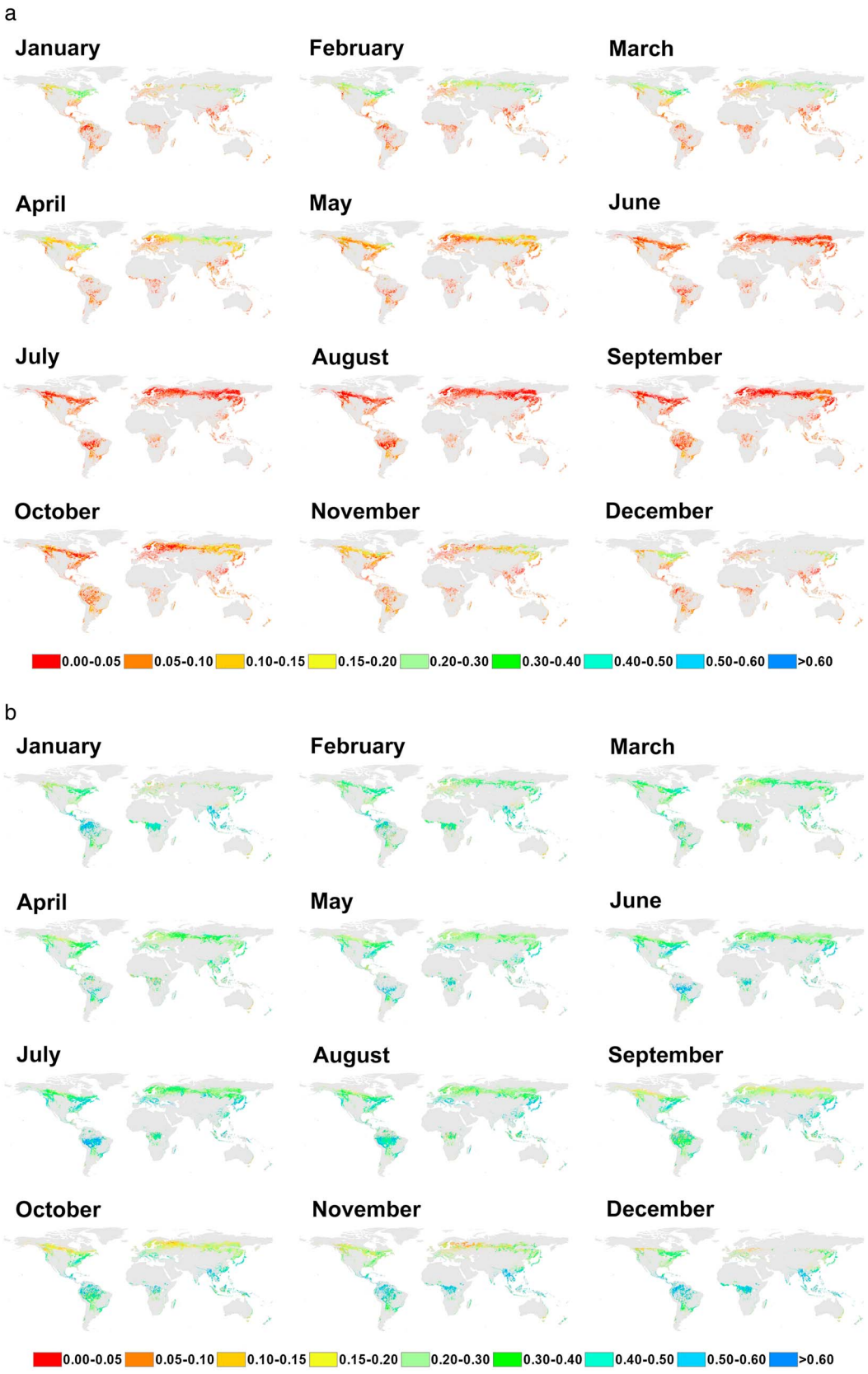

Figure 1. (a) Multi-year (from 2000 to 2010) monthly combined global background reflectivity in red band of MISR. (b) Multi-year (from 2000 to 2010) monthly combined global background reflectivity in NIR band of MISR.

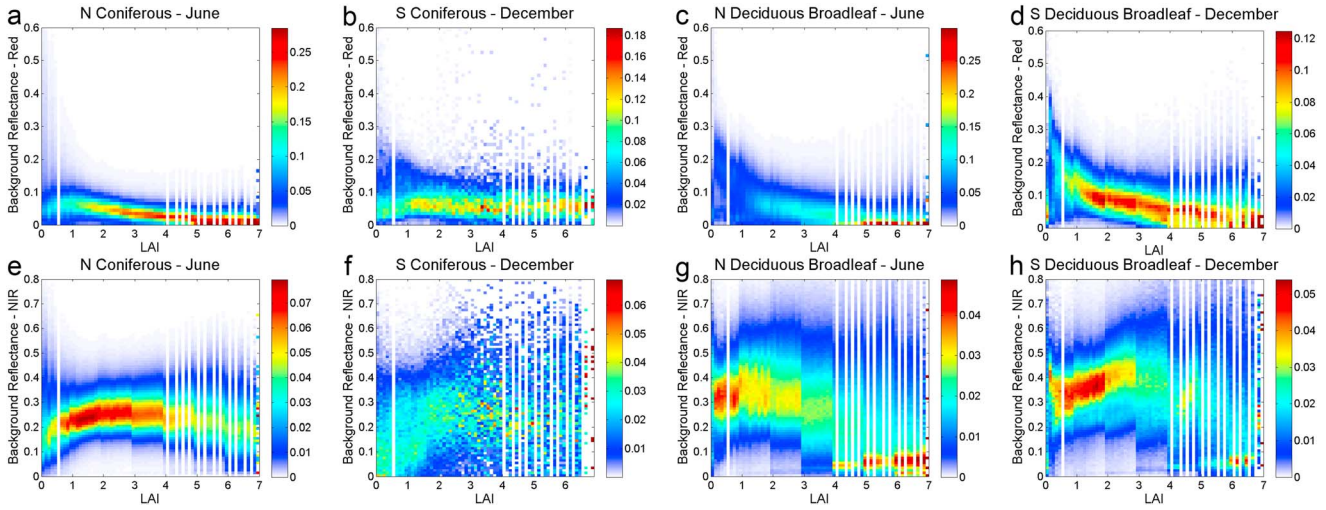

Figure 2. Distributions of background reflectivity in different LAI bins. The distribution of red reflectance for coniferous forest background in the (a) Northern and (b) Southern Hemispheres and for deciduous broadleaf forests background in the (c) Northern and (d) Southern Hemispheres, and the distribution of NIR reflectance for coniferous forest background in the (e) Northern and (f) Southern Hemispheres and for deciduous broadleaf forests background in the (g) Northern and (h) Southern Hemispheres. Some white vertical lines mean that there is no valid background reflectance result with corresponding LAI bins.

Differences in prevailing understory species caused by distinct forest types [*Barbier et al.*, 2008] may be responsible for this spatial difference. Controlled by changeable precipitation gradients, forest backgrounds in Southern Hemisphere demonstrate irregular patterns of NIR reflectance. Influenced by wet and dry seasons, the NIR reflectance reaches a high or low once or twice a year. For example, the background reflectance of deciduous broadleaf forest in the central of southern America (north of Argentina) will reach low values in summer and winter and high values in spring and autumn, which is in line with the dry and wet seasons in this region [*Dordel et al.*, 2011].

4.2. The Distribution of Background Reflectivity Under Different Canopy LAI

As the important composition of forest background, understory vegetations have significant contributions to the spectral properties of forest background. Thus, factors affecting the growth of understory plants such as canopy openness [*Ricard et al.*, 2003; *Strengbom et al.*, 2004] and stand conditions such as litter depth, mass, and soil moisture [*North et al.*, 2005; *Yu and Sun*, 2013] will change forest background reflectivity to some extent. These variations could be observed in the distribution of forest background reflectivity under different canopy LAI in June for Northern Hemisphere and December for Southern Hemisphere (Figure 2). Except for the southern coniferous forest stand, the other three stands all seem to have clear patterns of distribution. When the canopy LAI is lower than 1, it seems that the quality of stand and underlying soil is unfavorable for the growth of understory vegetation. Thus, backgrounds in such stands tend to have higher red reflectance and lower NIR reflectance. Ground measurements support this by showing that red reflectance in an infertile site is higher than that in a fertile site, while the opposite applies to the NIR reflectance [*Rautiainen et al.*, 2009]. However, in comparison to deciduous broadleaf forest background, coniferous forest background shows a lower red reflectance in this situation because mosses or lichens are better adapted to harsh environments than herbs [*Rees et al.*, 2004]. Field measurements on the leafless coniferous forest floor confirm the presence of a thick moss layer, which contains a great amount of chlorophyll per ground area that strongly absorbs radiation in the red band [*Hallik et al.*, 2009; *Suzuki et al.*, 2007]. Forest canopy LAI (2–3) increases with improved growing conditions but does not prevent sufficient sunlight from reaching the understory. Taking advantage of such stands, understory vegetation gradually dominates the floor, resulting in increased NIR reflectance and decreased red reflectance. A plateau is observed near LAI 3–4, indicating a seemingly stable development of understory vegetation that benefits from a sufficient amount of available light and precipitation. But when the canopy LAI is over 4, direct sunlight received by the forest floor drops dramatically, limiting the development of shade-intolerant plants [*Naumburg and DeWald*, 1999]. In addition, the shade-tolerant vegetation covers less and does not grow well in dense forest [*Roberts*, 1992]. Thus, the combination of these two factors leads to declining reflectance in

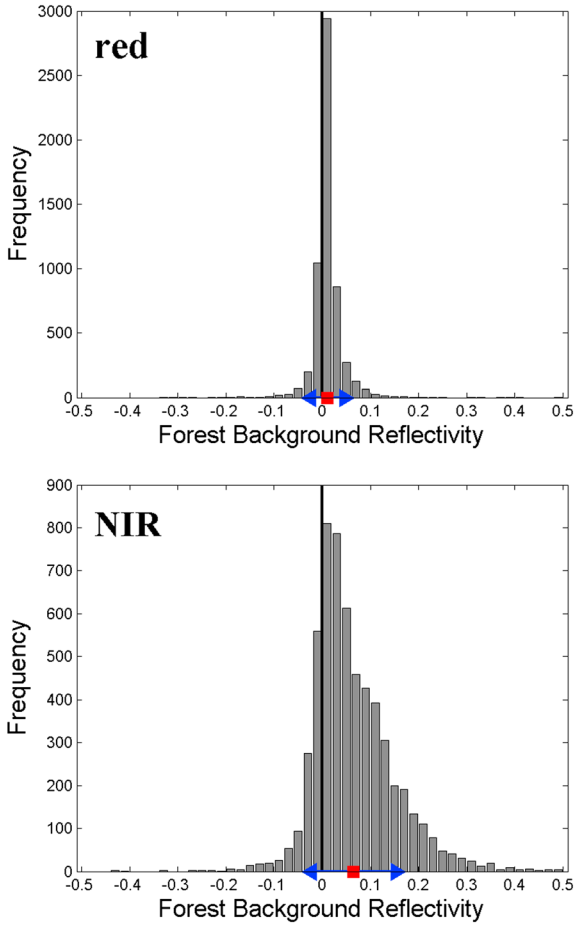

Figure 3. Distribution of differences between the deciduous broadleaf forest background and coniferous forest background in the red and NIR bands when both types of forests were found within the corresponding 1° pixel. Positive values signify lower values for coniferous forest. The position of red square in horizontal axis refers to the mean of their differences and the distance from blue triangle to the red square refers to the standard error of their differences.

the NIR band. Notably, coniferous forest background shows a smooth decline in NIR reflectance with increasing LAI, while a steep change is observed in NIR background reflectance for deciduous broadleaf forest at a threshold LAI. This difference is accounted for by the fact that high clumping of coniferous canopies allows more light to penetrate than for deciduous broadleaf forest canopies with the same LAI [*Rautiainen*, 2005].

4.3. Differences in Background Reflectivity Between Coniferous and Deciduous Broadleaf Forests

According to fields measurement reported in literature [*Barbier et al.*, 2008], the composition of understory vegetation in coniferous forests differs from broadleaf forests. Could this difference be expressed on the background reflectivity as well? To explore differences of background reflectivity between coniferous and deciduous broadleaf forests, two background reflectivity data sets over Northern Hemisphere at 1 decimal degree were created in each month by upscaling the 1 km resolution retrievals and combining results from multiyears (2000–2010). The first one is for coniferous forests only and the other one contains retrievals only for deciduous broadleaf forests. During the whole growing season, there are no significant differences between the two forest backgrounds in the red band with values normally distributing around zero. The differences in the NIR band between the upscaled background reflectivities from the two biomes are also normally distributed, but the deciduous broadleaf forest background reflectance tends to be larger than that of the coniferous forest in every month of the growing season, The most significant difference in the NIR occurs in September and is shown here together with the red band (Figures 3a and 3b). Our finding is in line with the field measurements of *Goward et al.* [1994], who observed broadleaf shrub and herbs with higher NIR reflectance dominating deciduous broadleaf forest whereas moss- and litter-covered coniferous forest background.

4.4. Comparison of Background Reflectivity With Grassland in the Vicinity

It is challenging to validate global forest background reflectivity due to the lack of systematic field measurements over large area. Based on the similar composition (e.g., herbs) and climatic conditions (e.g., light, precipitation, and temperature) between forest understory and its adjacent grassland, it is reasonable to assume that forest background shares a similar seasonal variation as its adjacent grassland. Therefore, a partial validation was carried by comparing retrieved background reflectivity with the nadir reflectance of grassland obtained from the MISR surface bidirectional reflectance product. Sample areas of more than 30,000 pixels for each forest type were selected over the Northern Hemisphere to make temporally coherent comparisons with grassland (Figures 4e–4h). And the corresponding grassland samples were picked by a 5×5 pixel window with a forest pixel centered. The comparisons show that background reflectivity patterns of all forest types are similar to their adjacent grasslands. During the whole growing season, background reflectance is closer to the reflectance of nearby grassland than to the total forest stand reflectance (Figures 4a–4h). However,

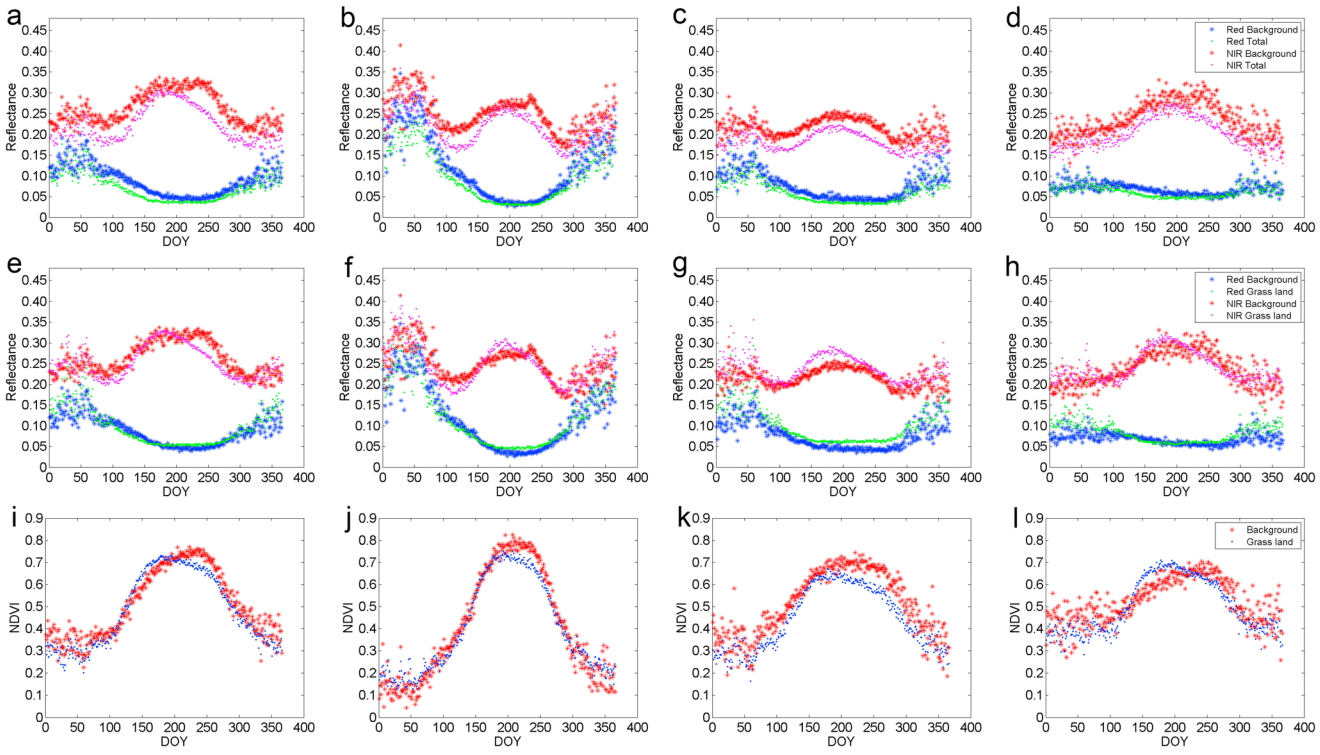

Figure 4. Temporal comparison between background reflectance and total reflectance, between background reflectance and grass land reflectance, between background NDVI and nearby grassland NDVI in Northern Hemisphere for four forest types: (a, e, and i) deciduous broadleaf forest, (b, f, and j) deciduous needleleaf forest, (c, g, and k) evergreen needleleaf forest, and (d, h, and l) evergreen broadleaf forest.

some differences in red and NIR reflectances tend to be enhanced when the normalized difference vegetation index (NDVI) is calculated (Figures 4i–4l). The steep increase of the grassland NDVI is in contrast to the slightly shallower rise of the broadleaf forest background NDVI in day of year (DOY) 50–180 (Figures 4i and 4l). This could be contributed to the distinct water and heat conditions caused by the covering of forest canopy developing at the same time period. Noticeably, this phenomenon disappears in the cases of needle leaf forest, suggesting that the shield effect of needleleaf forest canopy is not as significant as the broadleaf forest canopy in the green-up process (DOY 50–180). Another important difference observed in the NDVI time series (Figures 4i–4l) occurs in the climax of their growing seasons. Compared with adjacent grassland, understory vegetations for all forest types are shown to have extended growing season in the fall (DOY 180–250). This is consistent of the photosynthetic adaptation of understory vegetations such as shrub and herb, some of which tend to continue their growth by taking advantage of the favorable light conditions caused by leaf fall [*Jolly et al.*, 2004; *Katahata et al.*, 2005; *Rothstein and Zak*, 2001].

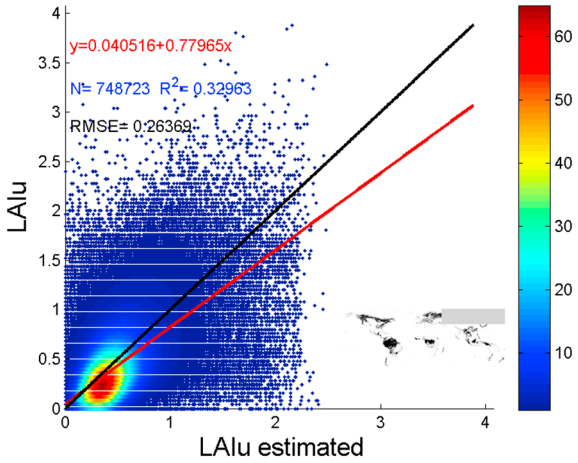

Figure 5. Comparison between understory LAI (LAIu) derived from background reflectances and the reference data set over larch forest region in North Asia (grey box) on the day of leaf appearance.

4.5. Comparison With Forest Understory LAI Over North Asia

Given the challenges of direct validation of forest background reflectivities, the understory LAI (LAIu) estimated from forest background reflectivities was compared with a reference data set [*Kobayashi et al.*, 2010] over the larch forest areas in North Asia (Figure 5). Based on

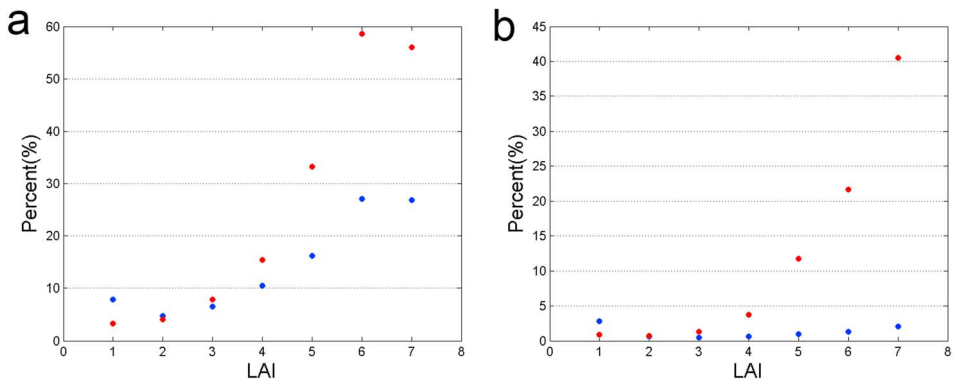

Figure 6. The failure (out normal range of reflectance (from 0 to 1)) percent of background reflectivity retrieval in different LAI for coniferous (blue dots) and deciduous broadleaf (red dots) forests. Medium summers for both hemispheres are chosen. (a) In the red band and (b) in the NIR band.

the assumption that forest background has similar composition as grassland, the LAIu here was retrieved from SR (simple ratio) of background by using the global LAI mapping algorithm [*Deng et al.*, 2006] combined with a technique of look-up table [*Liu et al.*, 2007]. The referenced LAIu values were derived through a simulated relationship with normalized difference water index (NDWI) [*Xiao et al.*, 2002] on the day of leaf appearance [*Delbart et al.*, 2005] when the understory is the dominant factor in controlling the total reflectance. Their comparison (Figure 5) shows a good agreement with points of high density dispersing along the 1:1 line especially in the LAIu range from 0 to 0.8. In fact, LAI for most understory vegetation in coniferous forests is generally lower than 1 according to the field measurements in literature [e.g., *Barr et al.*, 2004; *Nadezhdina et al.*, 2004; *Serbin et al.*, 2009; *Turner et al.*, 2004]. The root-mean-square error is 0.26, which is within the accuracy of LAI estimation from satellite data (around ±0.5) required by the *Global Climate Observing System* [2006] and far lower than the uncertainties of most global LAI products (around ±1) [*Garrigues et al.*, 2008]. The area with the highest density (dark red) strays slightly from the 1:1 line, indicating that the referenced LAIu is little smaller than our estimation. This may be attributed to the appearance of evergreen trees in larch stands which deduces the NDWI measurements and finally results in the underestimation of understory LAI [*Kobayashi et al.*, 2010].

4.6. Performance of the Background Reflectivity Retrieval Algorithm Under different Canopy LAI

As the possibility of observing forest background in forest with dense canopy is largely deduced in an oblique view angle, it is sometimes impossible to retrieve reasonable background reflectivity under larger LAI due to the limited accuracy in the estimation of the proportions for four components. The performance of the forest background reflectivity retrieval algorithm is examined under different canopy LAI for coniferous and deciduous broadleaf forests in June (Figures 6a and 6b). The failure percentage for deciduous broadleaf forest increases dramatically with increasing canopy LAI (Figure 6a). When canopy LAI < 4, its failure percentage is within 10%. Nevertheless, when LAI > 4, the percentage of failure retrieval seems to increase exponentially as a result of the low visibility of the background. In contrast, the algorithm performs better for coniferous forest background (Figure 6b), especially in the NIR band. The retrieval failure percentage is universally lower than 5% for coniferous forest background reflectance in the NIR band, indicating that the effect of canopy LAI is not as strong as in deciduous broadleaf forest because of high clumping. Red reflectance, however, always has a larger failure percentage than NIR reflectance in larger LAI. This may be explained by the difference in spectra response of vegetation (overstory or understory), i.e., high reflectance in infrared band and low value in red band. Under the same error of four proportions estimated from four-scale model, the retrieved reflectance has more probability to be positive when the total reflectance used for calculation is larger. Thus, there are more successful retrievals in the infrared band than in the red band.

4.7. The Spatial Coherence of Global Forest Background Reflectivity Maps

The eligibility of seasonal background reflectivity maps for global applications largely depends on its spatial coverage with valid retrieval. Multi-year monthly combined data with different quality flags were used to evaluate the spatial coherence of retrieved background reflectivity during the growing season (Table 2).

Table 2. The Spatial Coverage of Background Reflectivity Retrieval With Different Qualities

		Red			NIR		
Coverage %	Number of Pixel	High Quality	Valid	No Data	High Quality	Valid	No Data
EBF[a]	12038663	24.04	39.69	36.82	31.32	48.38	36.82
DBF[b]	6900023	64.85	88.85	7.41	73.89	91.35	7.41
ENF[c]	9704649	64.26	89.29	9.36	68.83	90.40	9.36
DNF[d]	3061914	77.23	91.97	7.82	80.10	92.16	7.82

[a]EBF: evergreen broadleaf forest.
[b]DBF: deciduous broadleaf forest.
[c]ENF: evergreen needleleaf forest.
[d]DNF: deciduous needleleaf forest.

The results show that both coniferous and deciduous broadleaf forest regions have approximately 70% pixels covered by high-quality retrievals and the valid retrievals are close to 90%, suggesting that the multi-year seasonal combined retrievals are capable of being used on a global scale. The retrieval success percentage is not so encouraging for evergreen broadleaf forest due to the lack of MISR surface data with clear air conditions. In fact, the number of 10 year monthly accumulated clear sky days is less than 5 for most of its locations.

5. Discussion

The atmospherically corrected satellite signal in a pixel with moderate or low spatial resolution is the combination of reflectance from the canopy and its background, so it is crucial to consider background reflectivity if accurate extractions of canopy biophysical parameters such as the LAI and the fraction of absorbed photosynthetically active radiation are to be done. Additionally, background reflectivity also provides information about the understory compositions. For instance, different soil fertilities could be distinguished by using the maximum amplitude of background reflectance change in a year because more fertile stands tend to have larger seasonal variation in reflectance [*Rautiainen et al.*, 2009]. When remote sensing is used to study the response of vegetation to climate change, background reflectance would make it possible to distinguish the response of the canopy from that of the background [*Doktor et al.*, 2009]. Because some of the understory may take advantage of phenological avoidance of canopy shade to develop earlier or defoliate later [*Augspurger et al.*, 2005; *Rothstein and Zak*, 2001], it is necessary to take the background into consideration in order to better monitor and understand the changes in the whole ecosystem. The global forest background reflectivity results described here are promising to such applications. However, uncertainties introduced by several factors, such as the architectural parameters of forests in the model, land cover, and land cover change, should be taken into consideration when the data set is utilized.

There are two main types of forest (coniferous and deciduous broadleaf) separated in the model used for this work while the land cover map provides four types of forests. Therefore, two broadleaf forests are assigned to share the given architectural parameters of deciduous broadleaf forest and two needleleaf forests are assigned to share that of coniferous forest (Table 1). Since the structure of evergreen broadleaf forest [*Feroz et al.*, 2006] dramatically differs from the general structural description of deciduous broadleaf forest, replacing the former with the latter will definitely cause estimation errors in the proportions of components, thus leading to unconvincing background reflectivities which most be excluded from detailed analysis. Retrieval results would be improved by using specific architectural parameters for each forest type in the model.

As the estimation of the proportions of the four components in a pixel is based on the structural parameters of a concrete forest type, the accuracy of background reflectivity depends on the MODIS global land cover map of 2001. Similarly, land cover change is a potential source of uncertainty. However, it is here assumed that land cover does not change much in forest regions from 2000 to 2010, an assumption which should introduce little uncertainty for most situations. If conversion occurs within different coniferous forests, such as from evergreen needleleaf forest to deciduous needleleaf forest, the retrieval is little affected due to similar structural parameters. If, for example, forests changes from broadleaf to coniferous forest, the influence of a different structure may become obvious in the retrieval of background reflectivity, though the chance of such a conversion is low in natural conditions. However, retrieval may be greatly affected if forests are destroyed, or change into other vegetation types, such as grassland or crops, because the stand structure

is totally changed. But these changes mainly appear in regions dominated by evergreen broadleaf forest, the background reflectivity of which should be excluded from future work.

There are some drawbacks in the global forest background reflectivity data set. First, retrieved reflectivities of forest background tend to be unrealistic (less than 0 or more than 1) when canopy LAI $>$ 4, and the percent of such background reflectivities for deciduous broadleaf forest is much larger than for the coniferous forest. Noticeably, the contribution of background reflectance to the overall reflectance in such circumstances is not significant. Another drawback is that the retrievals with high-quality cover around 70% of global coniferous and deciduous broadleaf forest areas, leaving approximately 30% of forest regions that require further processing. In fact, most of the invalid retrieval is due to unrealistic background reflectances caused by large initial LAI values. To be noticed, background reflectivity for stands with dense canopy could be assigned a suitable fixed value such for the retrieval of canopy biophysical parameters [*Pinty and Verstraete*, 1998]. Third, due to lack of spectral measurements of forest background for global areas on moderate scales, the estimated background reflectance is directly validated. However, the partial validation with adjacent grassland and the comparison of understory LAI on leaf appearance day both indicate the relative reliability of results.

6. Conclusion

Taking advantage of the multi-angle observations of the MISR, the four-scale model of *Chen and Leblanc* [1997] makes it possible to retrieve forest background reflectivities over large areas. Global forest background seasonal reflectivity maps are presented here for the first time. Compared with previous forest background reflectivity maps over North America forest areas [*Pisek and Chen*, 2009], the global seasonal maps in this study keep the original spatial resolution, 1.1 km, which makes it possible to illustrate more details of forest background reflectivity over local scales and perfectly fulfills the needs of various applications at moderate scales.

The derived background reflectivity illustrates the following characteristics:

1. Forest background reflectivities in high latitudes of Northern Hemisphere demonstrate the seasonal variation of background components from snow to vegetation to litter and back again. In contrast, the forest background reflectivities in the Southern Hemisphere are relatively stable due to the continued cover of understory vegetation in a year.
2. The red reflectance of the forest background may be used as an indicator of snow cover and the growth of understory vegetation while NIR reflectivity may be more suitable for indicating the start of senescence of understory vegetation since the red reflectance rises linearly while the NIR reflectance passes through a local minimum at the end of the growing season.
3. Background reflectivity changes with the canopy openness. High values in the red band and low values in the NIR band for lower LAI are primarily related to unfavorable growth conditions while for higher LAI this is mainly accounted by the amount of direct sunlight reaching forest floor.
4. The background reflectance of coniferous forest differs from that of deciduous broadleaf forest in the NIR band. This may be accounted by differences in prevailing understory vegetation species caused by different overstory species.

Future work is needed to generate more spatially coherent global forest background reflectivities to discover how the incorporation of background reflectance into global LAI algorithms can improve the estimation of canopy LAI.

Acknowledgments

This research was funded by the China 973 program (2010CB950701) and the National Natural Science Foundation of China (41171285). Jan Pisek was supported by Estonian Science Foundation grant PUT232 "EST-SEEDS." The MISR products were obtained from the NASA Langley Research Center Atmospheric Sciences Data Center (https://eosweb.larc.nasa.gov/order-data) and MODIS data from the Land Processes Distributed Active Archive Center (https://lpdaac.usgs.gov/). The GLOBMAP LAI series from 2000 to 2010 is available on (http://www.globalmapping.org/globalLAI). We also thank Hideki Kobayashi for providing the understory LAI data set and leaf appearance date data from 2000 to 2009. This product will be hosted on the GlobalMapping Web site (http://www.globalmapping.org/globalBackRefl) for free download.

References

Ahl, D. E., S. T. Gower, S. N. Burrows, N. V. Shabanov, R. B. Myneni, and Y. Knyazikhin (2006), Monitoring spring canopy phenology of a deciduous broadleaf forest using MODIS, *Remote Sens. Environ.*, *104*(1), 88–95.

Augspurger, C. K., and E. A. Bartlett (2003), Differences in leaf phenology between juvenile and adult trees in a temperate deciduous forest, *Tree Physiol.*, *23*(8), 517–525.

Augspurger, C. K., J. M. Cheeseman, and C. F. Salk (2005), Light gains and physiological capacity of understorey woody plants during phenological avoidance of canopy shade, *Funct. Ecol.*, *19*(4), 537–546.

Bacour, C., and F. M. Breon (2005), Variability of biome reflectance directional signatures as seen by POLDER, *Remote Sens. Environ.*, *98*(1), 80–95.

Barbier, S., F. Gosselin, and P. Balandier (2008), Influence of tree species on understory vegetation diversity and mechanisms involved - A critical review for temperate and boreal forests, *For. Ecol. Manage.*, *254*(1), 1–15.

Barr, A. G., T. A. Black, E. H. Hogg, N. Kljun, K. Morgenstern, and Z. Nesic (2004), Inter-annual variability in the leaf area index of a boreal aspen-hazelnut forest in relation to net ecosystem production, *Agric. For. Meteorol.*, *126*(3-4), 237–255.

Bicheron, P., M. Leroy, O. Hautecoeur, and F. M. Bréon (1997), Enhanced discrimination of boreal forest covers with directional reflectances from the airborne polarization and directionality of Earth reflectances (POLDER) instrument, *J. Geophys. Res.*, *102*(D24), 29,517–29,528, doi:10.1029/97JD01330.

Bothwell, G. W., E. G. Hansen, R. E. Vargo, and K. C. Miller (2002), The Multi-angle Imaging SpectroRadiometer science data system, its products, tools, and performance, *IEEE Trans. Geosci. Remote Sens.*, *40*(7), 1467–1476.

Boyle, W. A., and J. L. Bronstein (2012), Phenology of tropical understory trees: Patterns and correlates, *Rev. Biol. Trop.*, *60*(4), 1415–1430.

Brown, L., J. M. Chen, S. G. Leblanc, and J. Cihlar (2000), A shortwave infrared modification to the simple ratio for LAI retrieval in boreal forests: An image and model analysis, *Remote Sens. Environ.*, *71*(1), 16–25.

Canisius, F., and J. M. Chen (2007), Retrieving forest background reflectance in a boreal region from Multi-angle Imaging SpectroRadiometer (MISR) data, *Remote Sens. Environ.*, *107*(1-2), 312–321.

Chen, J. M., and J. Cihlar (1996), Retrieving leaf area index of boreal conifer forests using Landsat TM images, *Remote Sens. Environ.*, *55*(2), 153–162.

Chen, J. M., and S. G. Leblanc (1997), A four-scale bidirectional reflectance model based on canopy architecture, *IEEE Trans. Geosci. Remote Sens.*, *35*(5), 1316–1337.

Chen, J. M., and S. G. Leblanc (2001), Multiple-scattering scheme useful for geometric optical modeling, *IEEE Trans. Geosci. Remote Sens.*, *39*(5), 1061–1071.

Chen, J. M., X. Li, T. Nilson, and A. Strahler (2000), Recent advances in geometrical optical modelling and its applications, *Remote Sens. Rev.*, *18*(2-4), 227–262.

Chopping, M. J. (2008), Terrestrial applications of multiangle remote sensing, in *Advances in Land Remote Sensing: System, Modeling, Inversion and Application*, edited by S. Liang, pp. 95–144, Springer, Dordrecht, Netherlands.

Deering, D. W., T. F. Eck, and B. Banerjee (1999), Characterization of the reflectance anisotropy of three boreal forest canopies in spring–summer, *Remote Sens. Environ.*, *67*(2), 205–229.

Delbart, N., L. Kergoat, T. Le Toan, J. Lhermitte, and G. Picard (2005), Determination of phenological dates in boreal regions using normalized difference water index, *Remote Sens. Environ.*, *97*(1), 26–38.

Deng, F., J. M. Chen, S. Plummer, M. Z. Chen, and J. Pisek (2006), Algorithm for global leaf area index retrieval using satellite imagery, *IEEE Trans. Geosci. Remote Sens.*, *44*(8), 2219–2229.

Diner, D. J., J. C. Beckert, G. W. Bothwell, and J. I. Rodriguez (2002), Performance of the MISR instrument during its first 20 months in Earth orbit, *Geosci. Remote Sens., IEEE Trans.*, *40*(7), 1449–1466.

Diner, D. J., et al. (2005), The value of multiangle measurements for retrieving structurally and radiatively consistent properties of clouds, aerosols, and surfaces, *Remote Sens. Environ.*, *97*(4), 495–518.

Diner, D. J., et al. (1998), Multi-angle Imaging SpectroRadiometer (MISR) - Instrument description and experiment overview, *IEEE Trans. Geosci. Remote Sens.*, *36*(4), 1072–1087.

Doktor, D., A. Bondeau, D. Koslowski, and F. W. Badeck (2009), Influence of heterogeneous landscapes on computed green-up dates based on daily AVHRR NDVI observations, *Remote Sens. Environ.*, *113*(12), 2618–2632.

Dordel, J., B. Seely, and S. W. Simard (2011), Relationships between simulated water stress and mortality and growth rates in underplanted Toona ciliata Roem. in subtropical Argentinean plantations, *Ecol. Modell.*, *222*(17), 3226–3235.

Eriksson, H. M., L. Eklundh, A. Kuusk, and T. Nilson (2006), Impact of understory vegetation on forest canopy reflectance and remotely sensed LAI estimates, *Remote Sens. Environ.*, *103*(4), 408–418.

Feroz, S. M., A. Hagihara, and M. Yokota (2006), Stand structure and woody species diversity in relation to stand stratification in a subtropical evergreen broadleaf forest, Okinawa Island, *J. Plant Res.*, *119*(4), 293–301.

Garrigues, S., et al. (2008), Validation and intercomparison of global leaf area index products derived from remote sensing data, *J. Geophys. Res.*, *113*, G02028, doi:10.1029/2007JG000635.

Global Climate Observing System (2006), Systematic observation requirements for satellite-based products for climate: Supplemental details to the satellite-based component of the implementation plan for the Global Observing System for Climate in support of the UNFCCC, *GCOS-107(WMO/TD No. 1338)*, 99 pp.

Gemmell, F. (2000), Testing the utility of multi-angle spectral data for reducing the effects of background spectral variations in forest reflectance model inversion, *Remote Sens. Environ.*, *72*, 46–63.

Gonsamo, A., and P. Pellikka (2012), The sensitivity based estimation of leaf area index from spectral vegetation indices, *ISPRS J. Photogramm. Remote Sens.*, *70*, 15–25.

Goward, S. N., K. F. Huemmrich, and R. H. Waring (1994), Visible-near-infrared spectral reflectance of landscape components in Western Oregon, *Remote Sens. Environ.*, *47*(2), 190–203.

Hallik, L., O. Kull, T. Nilson, and J. Penuelas (2009), Spectral reflectance of multispecies herbaceous and moss canopies in the boreal forest understory and open field, *Can. J. Remote Sens.*, *35*(5), 474–485.

Heiskanen, J. (2006), Tree cover and height estimation in the Fennoscandian tundra-taiga transition zone using multiangular MISR data, *Remote Sens. Environ.*, *103*(1), 97–114.

Huete, A. R. (1988), A soil-adjusted vegetation index (SAVI), *Remote Sens. Environ.*, *25*(3), 295–309.

Jolly, W. M., R. Nemani, and S. W. Running (2004), Enhancement of understory productivity by asynchronous phenology with overstory competitors in a temperate deciduous forest, *Tree Physiol.*, *24*(9), 1069–1071.

Kaasalainen, S., and M. Rautiainen (2005), Hot spot reflectance signatures of common boreal lichens, *J. Geophys. Res.*, *110*, D20102, doi:10.1029/2005JD005834.

Katahata, S., M. Naramoto, Y. Kakubari, and Y. Mukai (2005), Photosynthetic acclimation to dynamic changes in environmental conditions associated with deciduous overstory phenology in Daphniphyllum humile, an evergreen understory shrub, *Tree Physiol.*, *25*(4), 437–445.

Kobayashi, H., N. Delbart, R. Suzuki, and K. Kushida (2010), A satellite-based method for monitoring seasonality in the overstory leaf area index of Siberian larch forest, *J. Geophys. Res.*, *115*, G01002, doi:10.1029/2009JG000939.

Lang, M., A. Kuusk, T. Nilson, T. Lükk, M. Pehk, and G. Alm (2002), Reflectance spectra of ground vegetation in sub-boreal forests, *Web page*. [Available at http://www.aai.ee/bgf/ger2600/Tartu Observatory, Estonia. 2 May.]

Leblanc, S. G., P. Bicheron, J. M. Chen, M. Leroy, and J. Cihlar (1999), Investigation of directional reflectance in boreal forests with an improved four-scale model and airborne POLDER data, *IEEE Trans. Geosci. Remote Sens.*, *37*(3), 1396–1414.

Li, X. W., and A. H. Strahler (1985), Geometric-optical modeling of a conifer forest canopy, *IEEE Trans. Geosci. Remote Sens.*, *23*(5), 705–721.

Liu, R., J. M. Chen, J. Liu, F. Deng, and R. Sun (2007), Application of a new leaf area index algorithm to China's landmass using MODIS data for carbon cycle research, *J. Environ. Manage.*, *85*(3), 649–658.

Liu, Y., R. G. Liu, and J. M. Chen (2012), Retrospective retrieval of long-term consistent global leaf area index (1981–2011) from combined AVHRR and MODIS data, *J. Geophys. Res.*, *117*, G04003, doi:10.1029/2012JG002084.

Miller, J. R., et al. (1997), Seasonal change in understory reflectance of boreal forests and influence on canopy vegetation indices, *J. Geophys. Res.*, *102*(D24), 29,475–29,482, doi:10.1029/97JD02558.
Nadezhdina, N., F. Tatarinov, and R. Ceulemans (2004), Leaf area and biomass of Rhododendron understory in a stand of Scots pine, *For. Ecol. Manage.*, *187*(2-3), 235–246.
Naumburg, E., and L. E. DeWald (1999), Relationships between Pinus ponderosa forest structure, light characteristics, and understory graminoid species presence and abundance, *For. Ecol. Manage.*, *124*(2-3), 205–215.
Nemani, R., L. Pierce, S. Running, and L. Band (1993), Forest ecosystem processes at the watershed scale - Sensitivity to remotely-sensed leaf area index estimates, *Int. J. Remote Sens.*, *14*(13), 2519–2534.
Neyman, J. (1939), On a new class of "contagious" distributions, applicable in entomology and bacteriology, *Ann. Math. Stat.*, *10*, 35–57.
Nilson, T., and U. Peterson (1994), Age-dependence of forest reflectance - Analysis of main driving factors, *Remote Sens. Environ.*, *48*(3), 319–331.
North, M., B. Oakley, R. Fiegener, A. Gray, and M. Barbour (2005), Influence of light and soil moisture on Sierran mixed-conifer understory communities, *Plant Ecolog.*, *177*(1), 13–24.
Peltoniemi, J. I., S. Kaasalainen, J. Näränen, M. Rautiainen, P. Stenberg, H. Smolander, S. Smolander, and P. Voipio (2005), BRDF measurement of understory vegetation in pine forests: Dwarf shrubs, lichen, and moss, *Remote Sens. Environ.*, *94*(3), 343–354.
Pinty, B., and M. M. Verstraete (1998), Modeling the scattering of light by homogeneous vegetation in optical remote sensing, *J. Atmos. Sci.*, *55*(2), 137–150.
Pinty, B., T. Lavergne, T. Kaminski, O. Aussedat, R. Giering, N. Gobron, M. Taberner, M. M. Verstraete, M. Vossbeck, and J. L. Widlowski (2008), Partitioning the solar radiant fluxes in forest canopies in the presence of snow, *J. Geophys. Res.*, *113*, D04104, doi:10.1029/2007JD009096.
Pisek, J., and J. M. Chen (2009), Mapping forest background reflectivity over North America with Multi-angle Imaging SpectroRadiometer (MISR) data, *Remote Sens. Environ.*, *113*(11), 2412–2423.
Pisek, J., J. M. Chen, K. Alikas, and F. Deng (2010), Impacts of including forest understory brightness and foliage clumping information from multiangular measurements on leaf area index mapping over North America, *J. Geophys. Res.*, *115*, G03023, doi:10.1029/2009JG001138.
Pisek, J., J. M. Chen, J. R. Miller, J. R. Freemantle, J. I. Peltoniemi, and A. Simic (2009), Mapping forest background reflectance in a boreal region using multiangle compact airborne spectrographic imager data, *IEEE Trans. Geosci. Remote Sens.*, *48*(1), 499–510.
Qi, J., A. Chehbouni, A. R. Huete, Y. H. Kerr, and S. Sorooshian (1994), A modified soil adjusted vegetation index, *Remote Sens. Environ.*, *48*(2), 119–126.
Rautiainen, M. (2005), Retrieval of leaf area index for a coniferous forest by inverting a forest reflectance model, *Remote Sens. Environ.*, *99*(3), 295–303.
Rautiainen, M., T. Nilson, and T. Lukk (2009), Seasonal reflectance trends of hemiboreal birch forests, *Remote Sens. Environ.*, *113*(4), 805–815.
Rautiainen, M., P. Stenberg, T. Nilson, and A. Kuusk (2004), The effect of crown shape on the reflectance of coniferous stands, *Remote Sens. Environ.*, *89*(1), 41–52.
Rautiainen, M., M. Mottus, P. Stenberg, and S. Ervasti (2008a), Crown envelope shape measurements and models, *Silva Fennica*, *42*(1), 19–33.
Rautiainen, M., M. Mottus, J. Heiskanen, A. Akujarvi, T. Majasalmi, and P. Stenberg (2011), Seasonal reflectance dynamics of common understory types in a northern European boreal forest, *Remote Sens. Environ.*, *115*(12), 3020–3028.
Rautiainen, M., J. Suomalainen, M. Mottus, P. Stenberg, P. Voipio, J. Peltoniemi, and T. Manninen (2007), Coupling forest canopy and understory reflectance in the Arctic latitudes of Finland, *Remote Sens. Environ.*, *110*(3), 332–343.
Rautiainen, M., M. Lang, M. Mottus, A. Kuusk, T. Nilson, J. Kuusk, and T. Lukk (2008b), Multi-angular reflectance properties of a hemiboreal forest: An analysis using CHRIS PROBA data, *Remote Sens. Environ.*, *112*(5), 2627–2642.
Rees, W. G., O. V. Tutubalina, and E. I. Golubeva (2004), Reflectance spectra of subarctic lichens between 400 and 2400 nm, *Remote Sens. Environ.*, *90*(3), 281–292.
Ricard, J. P., C. Messier, S. Delagrange, and M. Beaudet (2003), Do understory sapling respond to both light and below-ground competition?, A field experiment in a north-eastern American hardwood forest and a literature review, *Ann. For. Sci.*, *60*(8), 749–756.
Roberts, M. R. (1992), Stand development and overstory understory interactions in an aspen northern hardwoods stand, *For. Ecol. Manage.*, *54*(1–4), 157–174.
Rothstein, D. E., and D. R. Zak (2001), Photosynthetic adaptation and acclimation to exploit seasonal periods of direct irradiance in three temperate, deciduous-forest herbs, *Funct. Ecol.*, *15*(6), 722–731.
Roujean, J. L., M. Leroy, and P. Y. Deschamps (1992), A bidirectional reflectance model of the Earth's surface for the correction of remote sensing data, *J. Geophys. Res.*, *97*(D18), 20,455–20,468, doi:10.1029/92JD01411.
Sandmeier, S., and D. W. Deering (1999), Structure analysis and classification of boreal forests using airborne hyperspectral BRDF data from ASAS, *Remote Sens. Environ.*, *69*(3), 281–295.
Sellers, P. J., et al. (1997), Modeling the exchanges of energy, water, and carbon between continents and the atmosphere, *Science*, *275*(5299), 502–509.
Serbin, S. P., S. T. Gower, and D. E. Ahl (2009), Canopy dynamics and phenology of a boreal black spruce wildfire chronosequence, *Agric. For. Meteorol.*, *149*(1), 187–204.
Spanner, M. A., L. L. Pierce, D. L. Peterson, and S. W. Running (1990), Remote-sensing of temperate coniferous forest leaf-area index - The influence of canopy closure, understory vegetation and background reflectance, *Int. J. Remote Sens.*, *11*(1), 95–111.
Startsev, N., V. J. Lieffers, and S. M. Landhausser (2008), Effects of leaf litter on the growth of boreal feather mosses: Implication for forest floor development, *J. Veg. Sci.*, *19*(2), 253–260.
Strengbom, J., T. Nasholm, and L. Ericson (2004), Light, not nitrogen, limits growth of the grass Deschampsia flexuosa in boreal forests, *Can. J. Bot.-Rev. Can. Bot.*, *82*(4), 430–435.
Suzuki, K., J. Kubota, H. Yabuki, T. Ohata, and V. Vuglinsky (2007), Moss beneath a leafless larch canopy: Influence on water and energy balances in the southern mountainous taiga of eastern Siberia, *Hydrol. Process*, *21*(15), 1982–1991.
Suzuki, R., K. Yoshikawa, and T. C. Maximov (2001), Pheonological photographs of Siberian larch forest from 1997 to 2000 at Spasskaya Pad, Republic of Sakha, Russia, *Web page*. [Available at http://www.jamstec.go.jp/iorgc/hcorp/data/database/products/phenol/index.htm.]
Turner, M. G., D. B. Tinker, W. H. Romme, D. M. Kashian, and C. M. Litton (2004), Landscape patterns of sapling density, leaf area, and aboveground net primary production in postfire lodgepole pine forests, Yellowstone National Park (USA), *Ecosystems*, *7*(7), 751–775.
Wang, Y. J., et al. (2004), Evaluation of the MODIS LAI algorithm at a coniferous forest site in Finland, *Remote Sens. Environ.*, *91*(1), 114–127.

White, H. P., J. R. Miller, and J. M. Chen (2001), Four-scale linear model for anisotropic reflectance (FLAIR) for plant canopies - Part I: Model description and partial validation, *IEEE Trans. Geosci. Remote Sens.*, *39*(5), 1072–1083.

White, H. P., J. R. Miller, and J. M. Chen (2002a), Four-scale linear model for anisotropic reflectance (FLAIR) for plant canopies - Part II: Validation and inversion with CASI, POLDER, and PARABOLA data at BOREAS, *IEEE Trans. Geosci. Remote Sens.*, *40*(5), 1038–1046.

White, H. P., J. C. Deguise, J. Schwarz, R. Hitchcock, K. Staenz, and Ieee (2002b), *Defining Shaded Spectra by Model Inversion for Spectral Unmixing of Hyperspectral Datasets - Theory and Preliminary Application*, pp. 989–991, Ieee, New York.

Xiao, X. M., S. Boles, J. Y. Liu, D. F. Zhuang, and M. L. Liu (2002), Characterization of forest types in Northeastern China, using multi-temporal SPOT-4 VEGETATION sensor data, *Remote Sens. Environ.*, *82*(2-3), 335–348.

Yu, M., and O. J. Sun (2013), Effects of forest patch type and site on herb-layer vegetation in a temperate forest ecosystem, *For. Ecol. Manage.*, *300*, 14–20.